

Charmless b -meson and b -baryon decays at LHCb

Adam Morris*, on behalf of LHCb collaboration

University of Edinburgh

E-mail: adam.morris@cern.ch

Recent measurements of charmless b -hadron decays using 3 fb^{-1} of pp collisions at $\sqrt{s} = 7$ and 8 TeV , collected by the LHCb experiment, are presented. A search is performed for Λ_b and Ξ_b^0 decays to $\Lambda h^+ h'^-$ final states. The decays $\Lambda_b \rightarrow \Lambda K^+ \pi^-$ and $\Lambda_b \rightarrow \Lambda K^+ K^-$ are observed for the first time, and their branching fractions and CP asymmetries are measured. Evidence is seen for the $\Lambda_b \rightarrow \Lambda \pi^+ \pi^-$ channel, and limits are set on the branching fractions of the $\Xi_b^0 \rightarrow \Lambda h^+ h'^-$ decay modes. The decay $\Lambda_b \rightarrow \Lambda \phi$ is observed for the first time, and its branching fraction and T -odd triple-product asymmetries are measured. A search is performed for the decay $B_c^+ \rightarrow p \bar{p} \pi^+$. No signal is found, and an upper limit is set on the product of the branching fraction with the ratio of B_c^+ and B^+ production cross-sections.

XIII International Conference on Heavy Quarks and Leptons
22-27 May, 2016
Blacksburg, Virginia, USA

*Speaker.

1. Introduction

These proceedings detail recent results of measurements of charmless b -hadron decay modes, performed using data collected by the LHCb experiment during 2011 and 2012. Here, charmless b -hadron decays are defined as the decay of hadrons with non-zero beauty to fully hadronic final states that contain no b or c quarks. Where particles and decay processes are written, their charge conjugates are also implied, unless otherwise indicated.

1.1 Motivation

Charmless decays of b -hadrons can be divided into three categories: $b \rightarrow (s, d)$ flavour-changing neutral current (FCNC) transitions, $b \rightarrow u$ suppressed tree-level transitions and $b\bar{c} \rightarrow (d, s)\bar{u}$ annihilation processes. Since FCNC processes are forbidden at tree-level in the Standard Model, dominant diagrams for $b \rightarrow (s, d)$ transitions must contain a loop, which enhances the sensitivity of these decays to possible new physics effects. Tree-level $b \rightarrow u$ transitions are allowed, but are suppressed by a factor of the CKM matrix element V_{ub} . This means that the contribution from loop-level diagrams is similar in magnitude to that of tree-level. The tree and penguin diagrams have a relative weak phase γ , and their interference can lead to measurable CP violation. Charmless decays of $b\bar{c}$ states must proceed via annihilation diagrams, hence they can be used to probe charged propagators not present in the Standard Model.

1.2 Event selection

The dataset consists of proton-proton collisions, corresponding to an integrated luminosity of 3 fb^{-1} , of which 1 fb^{-1} was recorded at $\sqrt{s} = 7 \text{ TeV}$ and 2 fb^{-1} at $\sqrt{s} = 8 \text{ TeV}$. The LHCb detector is a single arm forward spectrometer, covering a range in pseudorapidity $2 < \eta < 5$, designed for precision studies of heavy quark decays [1, 2].

Signal candidate events are selected based on track quality, vertex quality and isolation criteria, as well as kinematic and topological information. Multivariate algorithms are trained to discriminate between signal and combinatorial background. Hadron particle identification requirements are imposed using information from the ring-imaging Cherenkov detectors, which distinguishes between pions, kaons and protons, in order to reduce misidentified backgrounds.

Charged tracks in the LHCb detector are classified under several categories depending on the sub-detectors that they pass through. Datasets can be split by track type, as the mass resolution will differ between them. The track types used in these analyses are “long”, which pass through all tracking stations, and “downstream”, which pass through all stations except the vertex locator. This is particularly important for the decay products of long-lived particles, such as Λ baryons and K_S^0 mesons.

2. Observations of $\Lambda_b \rightarrow \Lambda K^+ \pi^-$ and $\Lambda_b \rightarrow \Lambda K^+ K^-$ and searches for other Λ_b and Ξ_b^0 decays to $\Lambda h^+ h'^-$

To date, only a handful of charmless b -baryon decays have been observed: $\Lambda_b \rightarrow p\pi^-$, $\Lambda_b \rightarrow pK^-$ [3] and $\Lambda_b \rightarrow K_S^0 p\pi^-$ [4]. Evidence has also been seen for the decay $\Lambda_b \rightarrow \Lambda\eta$ [5]. This

analysis, published in [6], is a search for Λ_b and Ξ_b^0 decays to $\Lambda h^+ h'^-$ final states, where $h = \pi$ or K .

The signal candidates are separated using hadron PID information into three samples: $\Lambda\pi^+\pi^-$, $\Lambda K^\pm\pi^\mp$ and ΛK^+K^- . Note that while the $\Lambda K^\pm\pi^\mp$ sample contains all four combinations of charges, the results are calculated with the assumption that the contributions from the suppressed $\Lambda_b \rightarrow \Lambda K^- \pi^+$ and $\Xi_b \rightarrow \Lambda K^+ \pi^-$ modes are negligible. Due to changes in the trigger software during data taking, the samples are divided into three data-taking periods (2011, 2012a and 2012b). The data samples are also split by the track type of the Λ decay products, giving a total of six subsamples. Decays proceeding via the open charm intermediate states $\Lambda_c^+ \rightarrow \Lambda K^+$, $\Xi_c^+ \rightarrow \Lambda h^+$ and $D^0 \rightarrow h^+ h'^-$ are vetoed, however the decay mode $\Lambda_b \rightarrow \Lambda_c^+(\rightarrow \Lambda\pi^+)\pi^-$ is retained separately for normalisation.

The yields of signal, background and normalisation decay modes are determined using simultaneous fits to the b -baryon candidate invariant mass distributions in the six subsamples for each final state. The fit models contain components for the Λ_b and Ξ_b^0 signal, cross-feed backgrounds, partially-reconstructed backgrounds and combinatorial background. The combinations of the fits to all subsamples are shown in Figure 1.

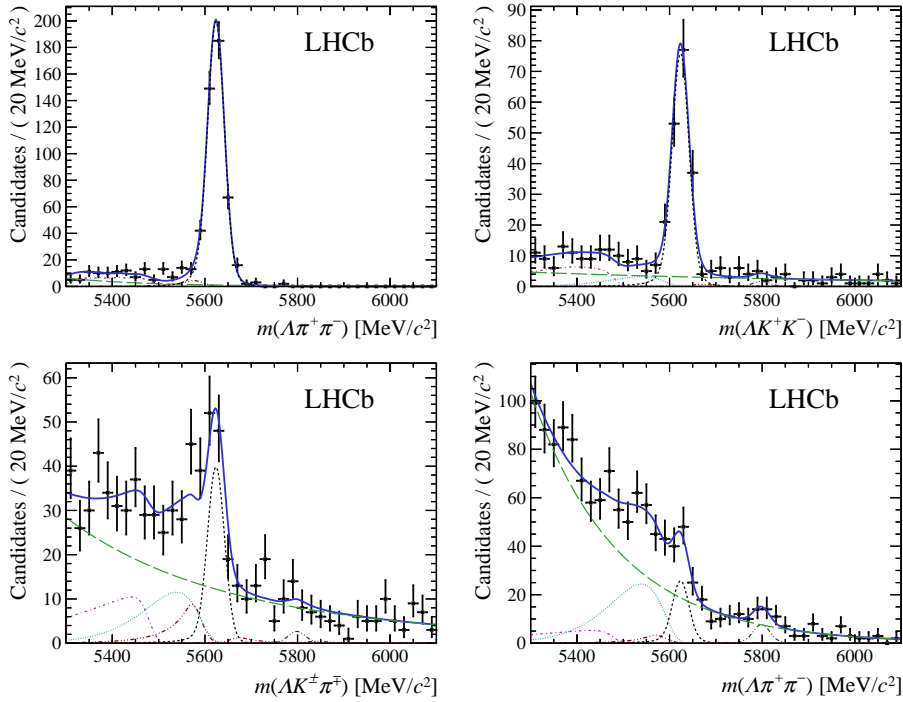


Figure 1: Invariant mass fits for the normalisation and signal modes. Upper left: fit to the $\Lambda_c^+(\rightarrow \Lambda\pi^+)\pi^-$ invariant mass. Upper right: fit to the ΛK^+K^- invariant mass. Lower left: fit to the $\Lambda K^\pm\pi^\mp$ invariant mass. Lower right: fit to the $\Lambda\pi^+\pi^-$ invariant mass. The total fit model is represented by the solid blue lines. The Λ_b and Ξ_b^0 components are represented by the short-dashed black and double dot-dashed grey lines, respectively. The cross-feed background is represented by the triple dot-dashed brown lines. The combinatorial background is represented by the long-dashed green lines. The partially reconstructed background with either a missing π^0 or γ are represented by dot-dashed purple lines or dotted cyan lines, respectively.

The signal selection efficiency can vary as a function of the five-dimensional phase space of

the decay, which is found to factorise into a two-dimensional Dalitz plot and three one-dimensional angular variables. Simulated events are used to calculate the selection efficiency as a function of these variables. When no signal is seen, the efficiency is taken as a simple average over the phase space. Where signals are observed, the efficiency is calculated using signal weights to make a weighted average over the phase space.

Sources of systematic uncertainty are the choice of fit model, simulation sample size, variation in efficiency across phase space, particle identification efficiency, mass vetoes for intermediate charm states and the uncertainty on the yield of the normalisation mode.

The decay modes $\Lambda_b \rightarrow \Lambda K^+ K^-$ and $\Lambda_b \rightarrow \Lambda K^+ \pi^-$ are observed for the first time, with significances of 15.8σ and 8.1σ respectively. Evidence is seen for the $\Lambda_b \rightarrow \Lambda \pi^+ \pi^-$, with a significance of 4.7σ . The Λ_b branching fractions are calculated as

$$\frac{\mathcal{B}(\Lambda_b \rightarrow \Lambda h^+ h'^-)}{\mathcal{B}(\Lambda_b \rightarrow \Lambda_c^+ (\rightarrow \Lambda \pi^+) \pi^-)} = \frac{N_{\Lambda_b \rightarrow \Lambda h^+ h'^-}}{N_{\Lambda_b \rightarrow \Lambda_c^+ (\rightarrow \Lambda \pi^+) \pi^-}} \frac{\varepsilon_{\Lambda_b \rightarrow \Lambda_c^+ (\rightarrow \Lambda \pi^+) \pi^-}}{\varepsilon_{\Lambda_b \rightarrow \Lambda h^+ h'^-}},$$

where \mathcal{B} is branching fraction, N is number of candidates and ε is efficiency. The measured values of the Λ_b branching fractions are

$$\begin{aligned} \mathcal{B}(\Lambda_b \rightarrow \Lambda \pi^+ \pi^-) &= (4.6 \pm 1.2 \pm 1.4 \pm 0.6) \times 10^{-6}, \\ \mathcal{B}(\Lambda_b \rightarrow \Lambda K^+ \pi^-) &= (5.6 \pm 0.8 \pm 0.8 \pm 0.7) \times 10^{-6}, \\ \mathcal{B}(\Lambda_b \rightarrow \Lambda K^+ K^-) &= (15.9 \pm 1.2 \pm 1.2 \pm 2.0) \times 10^{-6}, \end{aligned}$$

where the uncertainties are quoted in the order of statistical, systematic and normalisation.

Since the fragmentation fraction $f_{\Xi_b^0}$ is not known, the measured quantity for the Ξ_b^0 decay modes is

$$\frac{f_{\Xi_b^0}}{f_{\Lambda_b}} \frac{\mathcal{B}(\Xi_b^0 \rightarrow \Lambda h^+ h'^-)}{\mathcal{B}(\Lambda_b \rightarrow \Lambda_c^+ (\rightarrow \Lambda \pi^+) \pi^-)} = \frac{N_{\Xi_b^0 \rightarrow \Lambda h^+ h'^-}}{N_{\Lambda_b \rightarrow \Lambda_c^+ (\rightarrow \Lambda \pi^+) \pi^-}} \frac{\varepsilon_{\Lambda_b \rightarrow \Lambda_c^+ (\rightarrow \Lambda \pi^+) \pi^-}}{\varepsilon_{\Xi_b^0 \rightarrow \Lambda h^+ h'^-}}.$$

Since no Ξ_b^0 modes are observed, the following limits on the product of the branching fraction and the ratio of fragmentation fractions are set

$$\begin{aligned} \frac{f_{\Xi_b^0}}{f_{\Lambda_b}} \times \mathcal{B}(\Xi_b^0 \rightarrow \Lambda \pi^+ \pi^-) &< 1.7 \times 10^{-6}, \\ \frac{f_{\Xi_b^0}}{f_{\Lambda_b}} \times \mathcal{B}(\Xi_b^0 \rightarrow \Lambda K^- \pi^+) &< 0.8 \times 10^{-6}, \\ \frac{f_{\Xi_b^0}}{f_{\Lambda_b}} \times \mathcal{B}(\Xi_b^0 \rightarrow \Lambda K^+ K^-) &< 0.3 \times 10^{-6}. \end{aligned}$$

The number of candidates for the two observed modes are sufficient to allow for a measurement of their CP asymmetries. The yields of Λ_b and $\bar{\Lambda}_b$ decays are determined separately and then corrected using the efficiency taken from Dalitz plots. The raw CP asymmetries are calculated as

$$A_{CP}^{\text{raw}} = \frac{N_f^{\text{corr}} - N_{\bar{f}}^{\text{corr}}}{N_f^{\text{corr}} + N_{\bar{f}}^{\text{corr}}}$$

where N_f^{corr} ($N_{\bar{f}}^{\text{corr}}$) is the efficiency-corrected yield for Λ_b ($\bar{\Lambda}_b$).

The raw CP asymmetry includes production and detection asymmetries, which must be corrected for. Since the normalisation mode has the same b -hadron production asymmetry, a similar

detection asymmetry and is expected to have negligible CP violation, it can be used to make this correction.

$$\Delta A_{CP}(\Lambda_b \rightarrow \Lambda h^+ h'^-) = A_{CP}^{\text{raw}}(\Lambda_b \rightarrow \Lambda h^+ h'^-) - A_{CP}^{\text{raw}}(\Lambda_b \rightarrow \Lambda_c^+ (\rightarrow \Lambda \pi^+) \pi^-)$$

The measured CP asymmetries are

$$\begin{aligned} \Delta A_{CP}(\Lambda_b \rightarrow \Lambda K^+ \pi^-) &= -0.53 \pm 0.23 \pm 0.11, \\ \Delta A_{CP}(\Lambda_b \rightarrow \Lambda K^+ K^-) &= -0.28 \pm 0.10 \pm 0.07, \end{aligned}$$

where the first uncertainty is statistical, and the second is systematic. Both are consistent with the conservation of CP symmetry to within 3σ . Dominant contributions to the systematic uncertainty come from the uncertainty on the A_{CP}^{raw} of the normalisation mode, the choice of fit model and the uncertainty on the efficiency correction.

3. Observation of the $\Lambda_b \rightarrow \Lambda \phi$ decay

The decay $\Lambda_b \rightarrow \Lambda \phi$ is a flavour-changing neutral current $b \rightarrow s\bar{s}s$ transition, which is forbidden at tree-level in the Standard Model, hence the dominant diagram contains a loop. This transition in B^0 and B_s^0 decays is of particular interest as probes for sources of non-Standard Model CP violation. Previously studied modes include $B^0 \rightarrow \phi K_S^0$ [7, 8], $B^0 \rightarrow \phi K^{*0}$ [9] and $B_s^0 \rightarrow \phi \phi$ [10, 11], all of which have so far been consistent with the Standard Model.

In this analysis, published in [12], the aim is to make a first observation of the decay $\Lambda_b \rightarrow \Lambda \phi$ and measure its branching fraction and T -odd triple-product asymmetries. The decay mode $B^0 \rightarrow \phi K_S^0$ is used for normalisation. Candidate ϕ mesons are reconstructed from $K^+ K^-$ pairs, K_S^0 mesons from $\pi^+ \pi^-$ pairs, and Λ baryons from $p \pi^-$ pairs.

The number of signal mode candidates is found by performing a three-dimensional fit to the $\Lambda \phi$, $p \pi^-$ and $K^+ K^-$ invariant mass distributions. The fit model contains components for the $\Lambda_b \rightarrow \Lambda \phi$ signal mode, non-resonant $\Lambda_b \rightarrow \Lambda K^+ K^-$ decays, random $\Lambda \phi$ combinations and a purely combinatorial $K^+ K^- p \pi^-$ background. Separate fits are performed to candidates with long or downstream tracks from the Λ decay. The projections of the mass fits are shown in Figure 2.

In a similar manner, the number of normalisation mode candidates is found by fitting to the $K_S^0 \phi$, $\pi^+ \pi^-$ and $K^+ K^-$ invariant mass distributions. The fit model contains components for the $B^0 \rightarrow \phi K_S^0$ normalisation mode, non-resonant $B^0 \rightarrow K^+ K^- K_S^0$ decays, random combinations of $K^+ K^- K_S^0$ and a purely combinatorial $K^+ K^- \pi^+ \pi^-$ background. Separate fits are performed to candidates with long or downstream tracks from the K_S^0 decay. The projections of the mass fits are shown in Figure 3.

The total efficiency is the product of the reconstruction, selection, trigger and geometric detector acceptance, all of which are calculated using the simulation. The difference in detector material interaction cross section is determined from simulation. Data-driven corrections are applied where simulation disagrees with data. The hardware-level hadron trigger efficiency is corrected using calibration samples from charm decays. The reconstruction efficiency for long tracks is corrected with a tag-and-probe method with J/ψ calibration samples. The vertexing efficiency is corrected using calibration samples of $D^0 \rightarrow \phi K_S^0$ decays.

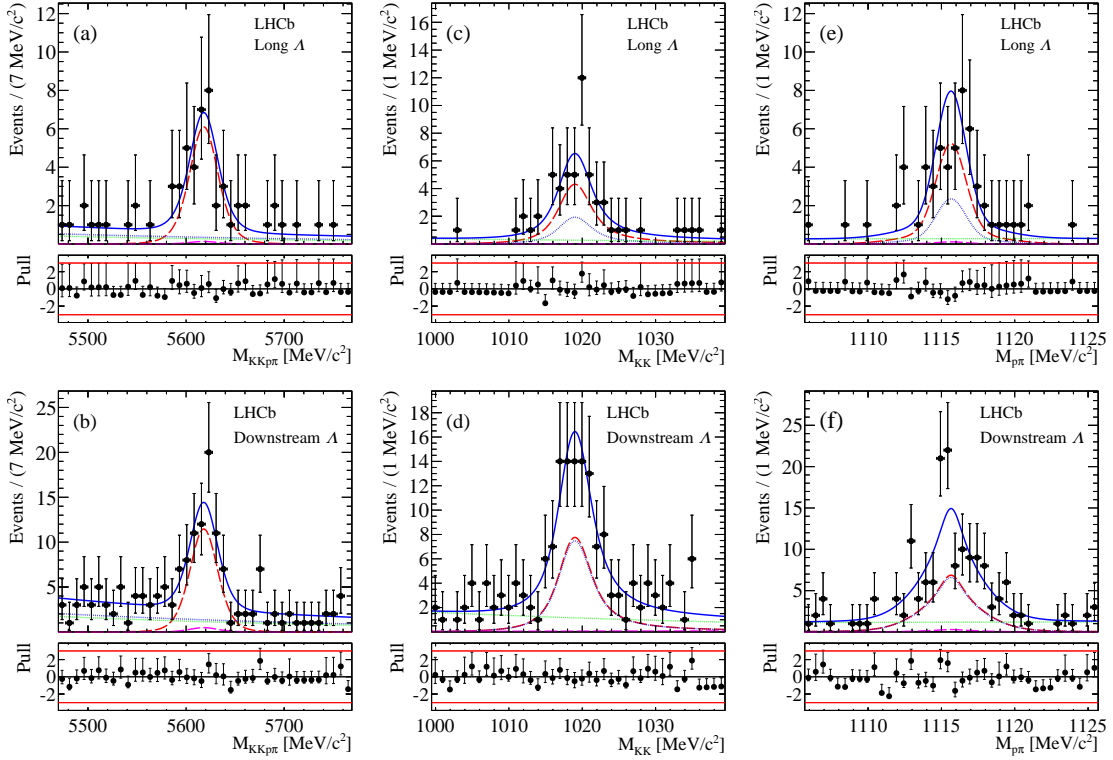


Figure 2: Fits to the (a and b) $\Lambda\phi$, (c and d) K^+K^- and (e and f) $p\pi^-$ invariant mass distributions. The upper row shows projections of the fit to the long Λ sample, and the lower row shows projections of the fit to the downstream Λ sample. The total fit is represented by the solid blue lines. The $\Lambda_b \rightarrow \Lambda\phi$ signal component is represented by the red dashed lines and the non-resonant $\Lambda_b \rightarrow \Lambda K^+K^-$ component by the magenta dashed lines. The random $\Lambda\phi$ combinations and a purely combinatorial $K^+K^-p\pi^-$ background components are represented by the blue and green dotted lines, respectively.

The largest sources of systematic uncertainty come from the selection efficiency, the choice of mass model, the hardware-level hadron trigger efficiency, the vertexing efficiency and the simulation sample size.

The decay $\Lambda_b \rightarrow \Lambda\phi$ is observed with a significance of 5.9σ . The branching fraction is calculated as

$$\mathcal{B}(\Lambda_b \rightarrow \Lambda\phi) = \frac{f_d}{f_{\Lambda_b}} \frac{N_{\Lambda_b \rightarrow \Lambda\phi}}{N_{B^0 \rightarrow \phi K_S^0}} \frac{\epsilon_{B^0 \rightarrow \phi K_S^0}}{\epsilon_{\Lambda_b \rightarrow \Lambda\phi}} \frac{\mathcal{B}(B^0 \rightarrow \phi K^0)}{2} \frac{\mathcal{B}(K_S^0 \rightarrow \pi^+\pi^-)}{\mathcal{B}(\Lambda \rightarrow p\pi^-)}.$$

The result of the $\Lambda_b \rightarrow \Lambda\phi$ branching fraction is

$$\mathcal{B}(\Lambda_b \rightarrow \Lambda\phi) = (5.18 \pm 1.04 \pm 0.35_{-0.43}^{+0.50} \pm 0.44) \times 10^{-6},$$

where the first uncertainty is statistical, the second systematic, the third from normalisation and the fourth from the ratio of fragmentation fraction f_d/f_{Λ_b} .

The $\Lambda_b \rightarrow \Lambda\phi$ decay is a transition from a spin- $\frac{1}{2}$ baryon to a spin- $\frac{1}{2}$ baryon plus a vector meson. Five decay angles are needed to describe the angular distributions of the decay, shown in Figure 4. The angle θ is the angle between the Λ momentum in the Λ_b rest frame with respect to the normal vector of the plane formed by the momentum vectors of the Λ_b and a beam proton. The

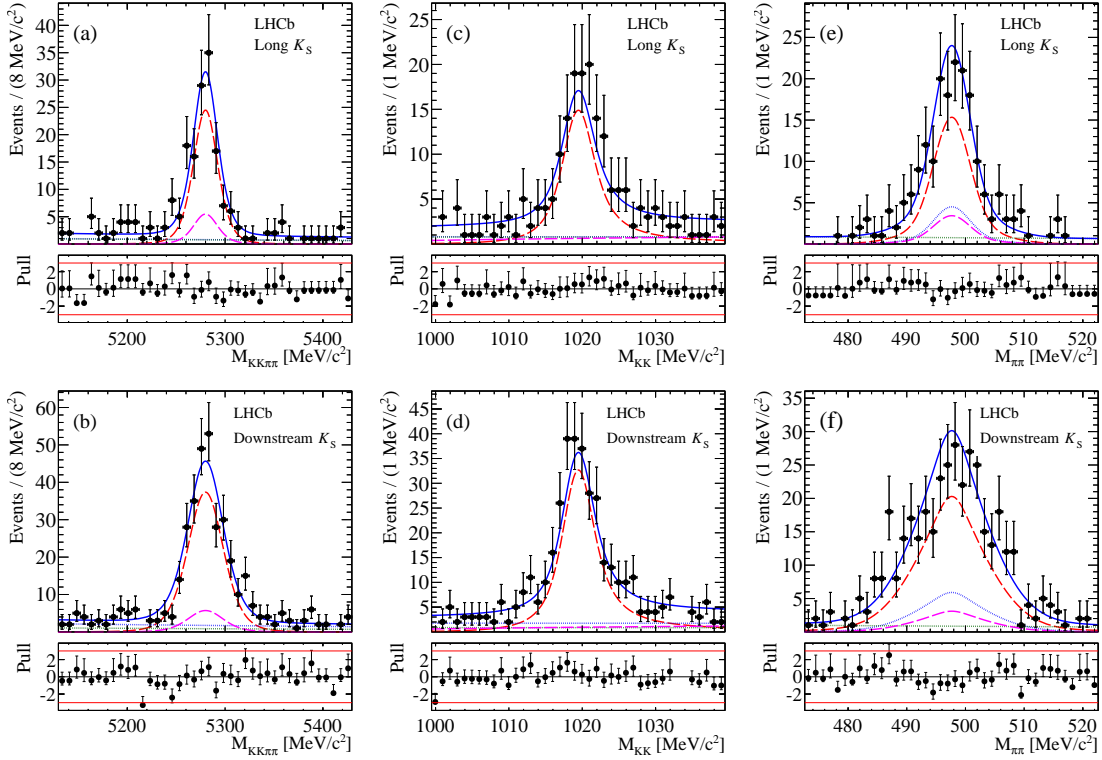


Figure 3: Fits to the (a and b) $K_S^0\phi$, (c and d) K^+K^- and (e and f) $\pi^+\pi^-$ invariant mass distributions. The upper row shows projections of the fit to the long K_S^0 sample, and the lower row shows projections of the fit to the downstream K_S^0 sample. The total fit is represented by the solid blue lines. The $B^0 \rightarrow \phi K_S^0$ signal component is represented by the red dashed lines and the non-resonant $B^0 \rightarrow K_S^0 K^+ K^-$ component by the magenta dashed lines. The random $K_S^0 K^+ K^-$ combinations and a purely combinatorial $K^+ K^- \pi^+ \pi^-$ background components are represented by the blue and green dotted lines, respectively.

angles θ_Λ and Φ_Λ are polar and azimuthal angles of the final state p in Λ rest frame. The angles θ_ϕ and Φ_ϕ are polar and azimuthal angles of the final state K^+ in ϕ rest frame.

Four T -odd observables are constructed with these angles: $\cos(\Phi_\Lambda)$, $\sin(\Phi_\Lambda)$, $\cos(\Phi_\phi)$ and $\sin(\Phi_\phi)$. For each observable O , the dataset is split by the sign of O , and mass fits are performed to obtain the yields $N_D^{\pm,O}$, where $D = \Lambda$ or ϕ , and \pm denotes the sign of O . The triple-product asymmetries are calculated as

$$A_D^O = \frac{N_D^{+,O} - N_D^{-,O}}{N_D^{+,O} + N_D^{-,O}}.$$

The measured values of the T -odd triple-product asymmetries are

$$\begin{aligned} A_\Lambda^c &= -0.22 \pm 0.12 \pm 0.06 \\ A_\Lambda^s &= +0.13 \pm 0.12 \pm 0.05 \\ A_\phi^c &= -0.01 \pm 0.12 \pm 0.03 \\ A_\phi^s &= -0.07 \pm 0.12 \pm 0.01 \end{aligned}$$

where the first uncertainty is statistical, and the second is systematic. All results are consistent with no asymmetry to within 2σ , and the dominant uncertainties are statistical. Systematic uncertainties

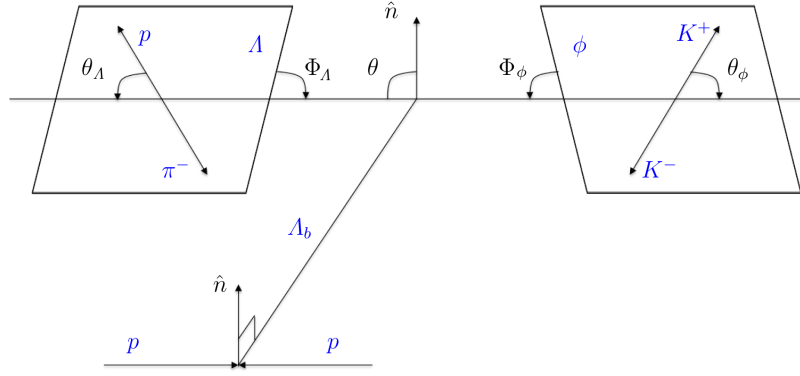


Figure 4: Decay angles for the $\Lambda_b \rightarrow \Lambda\phi$ decay.

arise from the choice of fit model, angular acceptance and resolution of the angular variables.

4. Search for B_c^+ decays to the $p\bar{p}\pi^+$ final state

Charmless decays of B_c^+ mesons proceed via annihilation diagrams, so can be used as a probe for new physics propagators, such as a charged Higgs. The amplitude of the leading order Feynman diagram for the process $\bar{b}c \rightarrow \bar{q}u$, where $q = d$ or s , is proportional to the product of CKM matrix elements $V_{cd}V_{uq}^*$. Therefore, due to Cabibbo suppression, final states with zero strangeness are the ones that dominate. In previous studies of B decays to final states containing baryon-antibaryon pairs, an enhancement is often seen at threshold, which is poorly understood [13, 14].

This analysis, published in [15], is a search for the decay $B_c^+ \rightarrow p\bar{p}\pi^+$ using $B^+ \rightarrow p\bar{p}\pi^+$ for normalisation. The focus is on $B_c^+ \rightarrow p\bar{p}\pi^+$ with $m(p\bar{p})$ below the $c\bar{c}$ production threshold, while the decay $B_c^+ \rightarrow J/\psi(\rightarrow p\bar{p})\pi^+$ is used as a cross check.

The dataset is divided into two regions of $p\bar{p}$ invariant mass: $m(p\bar{p}) < 2.85 \text{ GeV}/c^2$ for the charmless decays, and $2.85 < m(p\bar{p}) < 3.15 \text{ GeV}/c^2$ for $B_c^+ \rightarrow J/\psi(\rightarrow p\bar{p})\pi^+$. Fits are performed to the $p\bar{p}\pi^+$ invariant mass distributions with a model that contains components for $B_{(c)}^+ \rightarrow p\bar{p}\pi^+$, combinatorial background and partially reconstructed $B_{(c)}^+ \rightarrow p\bar{p}\rho^+(\rightarrow \pi^+\pi^0)$ with a missing π^0 .

The number of B_c^+ candidates in each $m(p\bar{p})$ region is found through simultaneous fits to the $p\bar{p}\pi^+$ invariant mass distributions in three bins of the multivariate classifier output. The fits to the most stringent bin are shown in Figure 5. The number of candidates found from the fit is consistent with zero.

The number of B^+ candidates in each $m(p\bar{p})$ region is found from fits to the $p\bar{p}\pi^+$ invariant mass distributions. The fits are shown in Figure 6. Only the region below the charmonium threshold is used for normalisation. The fit to the charmonium region shows a yield consistent with that observed in [16].

The overall detection efficiency ε is the product of the geometric detector acceptance and selection efficiency. Geometric detector acceptance is found from simulation. Selection efficiency is calculated using acceptance maps constructed on the $m^2(p\bar{p})$ vs $m^2(p\pi^+)$ plane. The effects of reconstruction, trigger, preselection and multivariate selection are modelled using simulation. The particle identification requirements are modelled by a data-driven technique using calibration

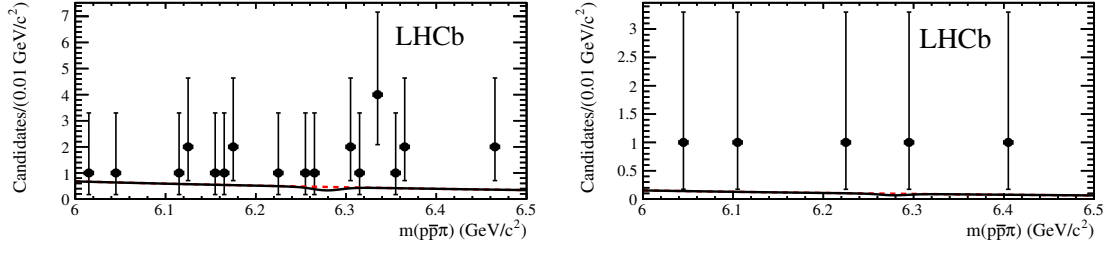


Figure 5: Fits to the $p\bar{p}\pi^+$ invariant mass in the highest bin of multivariate classifier output. The plot on the left is in the region $m(p\bar{p}) < 2.85 \text{ GeV}/c^2$, while the plot on the right is in the region $2.85 < m(p\bar{p}) < 3.15 \text{ GeV}/c^2$. The total fit is represented by the solid black lines. The combinatorial background is represented by the red long-dashed lines. The signal and partially reconstructed background components are too small to be shown.

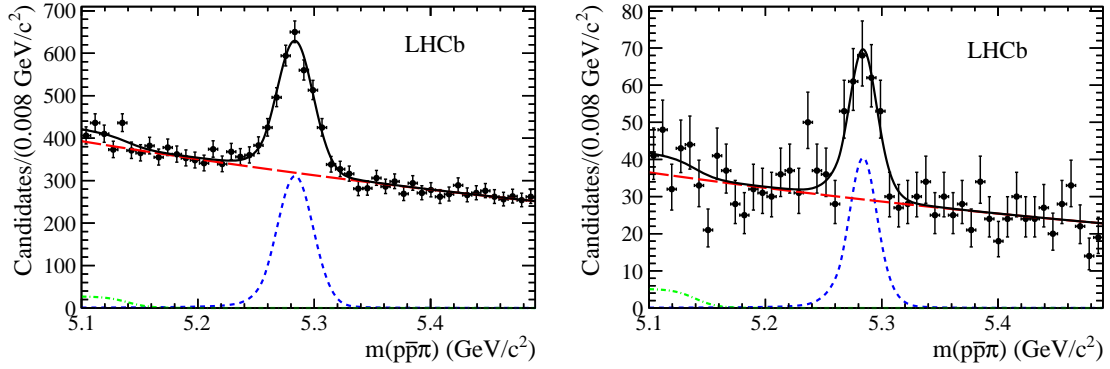


Figure 6: Fits to the $p\bar{p}\pi^+$ invariant mass. The plot on the left is in the region $m(p\bar{p}) < 2.85 \text{ GeV}/c^2$, while the plot on the right is in the region $2.85 < m(p\bar{p}) < 3.15 \text{ GeV}/c^2$. The total fit is represented by the solid black lines. The B^+ component is represented by a blue dashed line. The partially reconstructed background is represented by the green dot-dashed line. The combinatorial background is represented by the red long-dashed lines.

samples from charm decays. For the B^+ , signal weights are assigned to each candidate and used to calculate a weighted average for the efficiency over the acceptance map. Since no B_c^+ signal is seen in the data, a simple average is performed over the phase space region, which leads to a large systematic uncertainty. The ratio of selection efficiencies between the signal and normalisation channels is corrected for differences between data and simulation, such as tracking efficiency, hardware-level hadron trigger efficiency and fiducial region cuts.

The dominant sources of systematic uncertainties are the variation in the selection efficiency for $B_c^+ \rightarrow p\bar{p}\pi^+$ over the phase space region, the $B^+ \rightarrow p\bar{p}\pi^+$ branching fraction, the size of the proton calibration sample used in the particle identification map and the uncertainty in the B_c^+ lifetime.

Since the fragmentation fraction f_c is unknown, the measured quantities in this analysis are products of the branching fractions with the ratio of fragmentation fractions:

$$R_p \equiv \frac{f_c}{f_u} \mathcal{B}(B_c^+ \rightarrow p\bar{p}\pi^+) = \frac{N_{B_c^+ \rightarrow p\bar{p}\pi^+} \epsilon_u}{N_{B^+ \rightarrow p\bar{p}\pi^+} \epsilon_c} \mathcal{B}(B^+ \rightarrow p\bar{p}\pi^+),$$

and

$$R_p^{J/\psi} \equiv \frac{f_c}{f_u} \mathcal{B}(B_c^+ \rightarrow J/\psi \pi^+) = \frac{N_{B_c^+ \rightarrow J/\psi(\rightarrow p\bar{p})\pi^+}}{N_{B^+ \rightarrow p\bar{p}\pi^+}} \frac{\varepsilon_u}{\varepsilon_c^{J/\psi}} \frac{\mathcal{B}(B^+ \rightarrow p\bar{p}\pi^+)}{\mathcal{B}(J/\psi \rightarrow p\bar{p})},$$

where \mathcal{B} is branching fraction, N is number of candidates and ε is efficiency.

In order to set limits on R_p and $R_p^{J/\psi}$, profile likelihood ratio scans of these values are performed for the signal + background and background-only hypotheses. Signal p -values are calculated by dividing the signal + background p -values by the background-only p -values. The signal p -value scans for the two $m(p\bar{p})$ regions are shown in Figure 7. The point at which the signal p -value falls below 10% is taken as the upper limit at 90% confidence level.

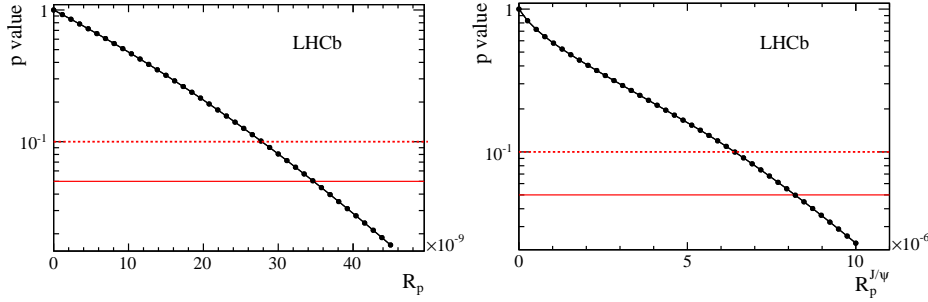


Figure 7: Left: p -value profile for R_p . Right: p -value profile for $R_p^{J/\psi}$. The horizontal solid and dashed red line indicate the 5% and 10% confidence levels, respectively.

The measured upper limits at 90% confidence level are

$$R_p < 2.8 \times 10^{-8},$$

and

$$R_p^{J/\psi} < 6.5 \times 10^{-6}.$$

5. Summary

Several recent measurements of charmless b -hadron decays, using the 2011 and 2012 proton-proton collision data sample collected by LHCb, have been presented.

In a search for charmless decays of Λ_b and Ξ_b^0 baryons to $\Lambda h^+ h'^-$ final states, the modes $\Lambda_b \rightarrow \Lambda K^+ \pi^-$ and $\Lambda_b \rightarrow \Lambda K^+ K^-$ are observed for the first time. Their branching fractions are measured relative to that of the decay $\Lambda_b \rightarrow \Lambda_c^+ (\rightarrow \Lambda \pi^+) \pi^-$. The CP asymmetries of the observed modes are found to be less than 3σ away from zero. Evidence is seen for the $\Lambda_b \rightarrow \Lambda \pi^+ \pi^-$ channel, and a measurement of its branching fraction is made. No evidence is seen for any of the $\Xi_b^0 \rightarrow \Lambda h^+ h'^-$ decay modes, and limits on their branching fractions are set.

The decay $\Lambda_b \rightarrow \Lambda \phi$ is observed for the first time, and its branching fraction is measured relative to that of the decay $B^0 \rightarrow \phi K_S^0$. The T -odd triple-product asymmetries of the $\Lambda_b \rightarrow \Lambda \phi$ decay mode are found to be consistent with zero.

A search for decays of the B_c^+ meson to the $p\bar{p}\pi^+$ final state is performed in two regions of $p\bar{p}$ invariant mass. No signal is observed, and limits are set on quantities corresponding to the branching fraction in each region multiplied by the ratio of fragmentation fractions f_c/f_u .

References

- [1] LHCb Collaboration, *The LHCb Detector at the LHC*, *JINST* **3** (2008) S08005
- [2] LHCb Collaboration, *LHCb Detector Performance*, *Int. J. Mod. Phys. A* **30** (2014) 1530022 [hep-ex/1412.6352]
- [3] CDF Collaboration, *Observation of New Charmless Decays of Bottom Hadrons*, *Phys. Rev. Lett.* **103** (2009) 031801 [hep-ex/0812.4271]
- [4] LHCb Collaboration, *Searches for Λ_b^0 and Ξ_b^0 decays to $K_S^0 p \pi^-$ and $K_S^0 p K^-$ final states with first observation of the $\Lambda_b^0 \rightarrow K_S^0 p \pi^-$ decay*, *JHEP* **04** (2014) 087 [hep-ex/1402.0770]
- [5] LHCb Collaboration, *Search for the $\Lambda_b^0 \rightarrow \Lambda \eta'$ and $\Lambda_b^0 \rightarrow \Lambda \eta$ decays with the LHCb detector*, *JHEP* **09** (2015) 006 [hep-ex/1505.03295]
- [6] LHCb Collaboration, *Observations of $\Lambda_b^0 \rightarrow \Lambda K^+ \pi^-$ and $\Lambda_b^0 \rightarrow \Lambda K^+ K^-$ decays and searches for other Λ_b^0 and Ξ_b^0 decays to $\Lambda h^+ h^-$ final states*, *JHEP* **05** (2016) 081 [hep-ex/1603.00413]
- [7] Belle Collaboration, *Measurement of time dependent CP violating asymmetries in $B^0 \rightarrow \phi K_S^0$, $K^+ K^- K_S^0$, and $\eta' K_S^0$ decays*, *Phys. Rev. Lett.* **91** (2003) 261602 [hep-ex/0308035]
- [8] BaBar Collaboration, *Study of CP violation in Dalitz-plot analyses of $B^0 \rightarrow K^+ K^- K_S^0$, $B^+ \rightarrow K^+ K^- K^+$ and $B^+ \rightarrow K_S^0 K_S^0 K^+$* , *Phys. Rev.* **D85** (2012) 112010 [hep-ex/1201.5897]
- [9] LHCb Collaboration, *Measurement of polarization amplitudes and CP asymmetries in $B^0 \rightarrow \phi K^*(892)^0$* , *JHEP* **05** (2014) 069 [hep-ex/1403.2888]
- [10] LHCb Collaboration, *First measurement of the CP-violating phase in $B_s^0 \rightarrow \phi \phi$ decays*, *Phys. Rev. Lett.* **110** (2013) 241802 [hep-ex/1303.7125]
- [11] LHCb Collaboration, *Measurement of CP violation in $B_s^0 \rightarrow \phi \phi$ decays*, *Phys. Rev.* **D90** (2014) 052011 [hep-ex/1407.2222]
- [12] LHCb Collaboration, *Observation of the $\Lambda_b \rightarrow \Lambda \phi$ decay*, *Phys. Lett.* **B759** (2016) 282 [hep-ex/1603.02870]
- [13] BaBar Collaboration, *Observation of the decay $\bar{B}^0 \rightarrow \Lambda_c^+ \bar{p} \pi^0$* , *Phys. Rev.* **D82** (2010) 031102 [hep-ex/1007.1370]
- [14] BaBar Collaboration, *Study of $e^+ e^- \rightarrow \Lambda \bar{\Lambda}$, $\Lambda \bar{\Sigma}^0$, $\Sigma^0 \bar{\Sigma}^0$ using initial state radiation with BaBar*, *Phys. Rev.* **D76** (2007) 092006 [hep-ex/0709.1988]
- [15] LHCb Collaboration, *Search for B_c decays to the $p \bar{p} \pi$ final state*, *Phys. Lett.* **B759** (2016) 313 [hep-ex/1603.07037]
- [16] LHCb Collaboration, *Evidence for CP Violation in $B^+ \rightarrow p \bar{p} K^+$ Decays*, *Phys. Rev. Lett.* **113** (2014) 141801 [hep-ex/1407.5907]